Load versus displacement-controlled nanocompression: Insights from atomistic simulations

Hugo Iteney, Thomas W Cornelius, Olivier Thomas, Jonathan Amodeo

H. Iteney, T.W. Cornelius, O. Thomas, J. Amodeo, Load versus displacement-controlled nanocompression: Insights from atomistic simulations, Scripta Mater. 226 (2023) 115245. https://doi.org/10.1016/j.scriptamat.2022.115245.

Load versus displacement-controlled nanocompression: insights from atomistic simulations

Hugo Iteney[a], Thomas W. Cornelius[a], Olivier Thomas[a], Jonathan Amodeo[a,b]

[a] *Aix-Marseille Université, Université de Toulon, CNRS, IM2NP, Marseille, 13013, France*
[b] *Univ Lyon, CNRS, INSA Lyon, UCBL, MATEIS, UMR5510, Villeurbanne, 69621, France*

Abstract

The mechanics of nano-objects strongly depends on the experimental setup used. Indeed, experimental devices generate stress either by controlling the force exerted by the grips (or indenters) or by monitoring their displacements, while software-based feedback loops are also developed to control displacements using force actuators. Often, nanomechanical experiments are interpreted using intrinsically displacement-controlled molecular dynamics simulations, without questioning the influence of the control mode. In this study, we develop an original strategy to perform load-controlled molecular dynamics simulations applied here to nanoparticles under compression as a test-case. While displacement-controlled simulations show intermittent plasticity and load drops, load-controlled simulations are characterized by strain-bursts more in line with load-controlled experiments. Here, a special attention is paid to the dislocation microstructure evolution depending on the control mode. Finally, interpretations of recent experiments based on atomistic simulations are revised, including the envelope load model usually used to correlate displacement-controlled atomistic simulations and load-controlled experiments at small-scales.

Keywords: Nanomechanics, molecular dynamics, load vs. displacement-control, nanoparticles

*Corresponding author
Email address: jonathan.amodeo@cnrs.fr (Jonathan Amodeo)

Only few methods exist to probe mechanical properties at small-scales including nanoindentation (maybe the most common), micro- and nanocompression as well as tensile tests [1, 2]. These techniques are either force-controlled (*i.e.,* driven by actuators that apply forces) or displacement-controlled. Two kinds of displacement-controlled tests currently exist. On the one hand, the most commonly used mode is the pseudo displacement-controlled mode where a feedback control algorithm such as the Proportional-Integral-Derivative (PID) is used to monitor displacements via a force actuator setup with more or less precision [3]. On the other hand, true displacement-controlled setups drive the displacements of grips or indenters based on the high-stiffness of fast-response piezoelectric actuators. One can notice that true displacement-controlled devices still suffer from the self-compliance of the load cell despite significant improvements in recent years [4]. In small-scale compression tests, open-loop force-controlled and pseudo displacement-controlled tests are easily recognizable from intrinsic displacement-controlled ones when looking at the load *vs.* displacement curves. This is particularly true when the mechanical response reaches the plastic deformation regime characterized by large displacement bursts (load-controlled or pseudo displacement-controlled cases) or sudden load drops (true displacement-controlled case). When applied to the study of NPs under compression, both methods are used without having clearly identified the role of the control mode on the load response or sample shape evolution [5, 6, 7, 8]. On the other hand, Molecular Dynamics (MD) simulations are also used to explore the mechanics of nano-objects [9, 10]. MD allows to identify the elementary deformation processes occurring during mechanical tests (not always observed experimentally) as well as a qualitative evaluation of the yield stress. From a simulation point of view, force-field indenters or frozen boundary atoms are displaced as a function of time to mimic experimental boundary conditions. The MD nanomechanical simulations are therefore inherently displacement-controlled, which does not preclude their use to discuss load-controlled experiments. While most collaborative studies do not comment on the control mode mismatch between experiments and MD, an envelope load model is often used to compare MD displacement-controlled simulations and load-controlled experiments and to justify the occurrence of strain bursts [5, 11, 12, 13]. Whereas one can argue on the validity of such an approach, a more general question arises about the pros and cons of exclusively using MD displacement-controlled simulations to interpret any type of nanomechanical experiments.

In this study, we develop an original approach to run load-controlled MD virtual experiments and use it to discuss the main differences between load- and displacement-controlled tests in the context of recent experiments and simulations performed on metal gold and silver NPs.

Here, MD simulations are performed using the open-source code LAMMPS [14] where Au and Ag atomic interactions are described respectively using the Grochola *et al.* [15] and the Zhou *et al.* [16] embedded-atom method (EAM) parameterizations. The transferability of these two potentials to nanomechanics is addressed in several studies in which computed lattice, surface and dislocation properties were shown to accurately reproduce experimental and DFT results [15, 16, 5, 13]. Wulff-shaped Au NPs with characteristic height ranging from 7.52 to 22.56 nm are designed using the Python WulffPack package [17] including low-index surface energies $\gamma_{\{100\}}$=1296.5, $\gamma_{\{110\}}$=1531.2 and $\gamma_{\{111\}}$=1196.4 mJ.m^{-2} as inputs (see supplementary information for computational details). In addition, 20.1 nm size Ag half-spheres are designed using Atomsk [18]. After sample design, the system is equilibrated at low temperature following a classical procedure described in Refs. [7, 19]. For nanocompression simulations, two infinite planar force fields are used respectively as indenter and sample substrate. The upper indenter is displaced towards the NP like a flat punch axis-aligned with the z=[111] direction while the lower force field is held fixed to support the sample. Here, we use $F_{ff,j} = -K(z_j - z_{ff})^2$ for the two force fields where $F_{ff,j}$ is applied to the atom j, z_j and z_{ff} referring respectively to the atom j and force field z coordinates. The force field constant K is imposed high enough (1000 eV.Å^{-3}) to limit the penetration of both the indenter and the substrate into the NP. During compression, the total indenter force $F_{ind} = \sum_{j=1}^{N} F_{ind,j}$, with N the number of atoms above the flat punch, is recorded *on-the-fly*. It allows to compute the engineering compressive stress $\sigma = F_{ind}/S_0$ where S_0 is the initial contact surface calculated using a convex Hull approach. The engineering strain is computed as the maximum relative variation of the NP height along the [111] compression direction $\varepsilon = \Delta l^{[111]}/l_0^{[111]}$.

Two types of compression control setups are used. On the one hand, the usual MD displacement-controlled approach relies on changing the indenter position z_{ind} iteratively at a constant displacement rate $\dot{\Delta l}$ using Equation 1.

$$z_{ind}(\dot{\Delta l}, t) = l_0(1 - \frac{\dot{\Delta l}}{l_0}t) \tag{1}$$

On the other hand, an original load-controlled simulation setup inspired by the experimental feedback concept is built using a Python solver as a feedback loop. Here, the indenter displacement is actuated to adjust the indenter force (and not the other way around). The Python solver is called at time interval Δt by the main MD script to force the match between the integrated user-imposed load rate $\dot{F}$ and the effective indenter force F_{ind}. The updated indenter position $z_{ind}(\dot{F}, t)$ is computed solving Equation 2. It can be noted that this feedback approach is extensible to any indenter shape as long as the group of atoms to which the indenter force is applied is properly defined. In the following, Δt is equal to the MD timestep δt (Δt=δt=2 fs) *i.e.,* we only focus here on comparing ideal displacement-controlled compression tests with load-controlled cases, without quantifying the influence of the machine compliance (see supplementary information for additional applications).

$$\dot{F}.\Delta t = \Delta F_{ind} \tag{2}$$

Using a harmonic force expression for $F_{ind,j}$, Equation 2 leads to two possible solutions $z_{ind}(\dot{F}, t)$=$\bar{z_j} \pm \Delta z_{ind}$ for which only the lowest polynomial root ensures the monotonous increase of F_{ind}. Under load control, the updated position of the indenter is provided by Equation 3.

$$z_{ind}(\dot{F}, t) = \frac{1}{N}\sum_{j=1}^{N} z_j - \frac{1}{N}\sqrt{\left(\sum_{j=1}^{N} z_j\right)^2 + N\left(\frac{\dot{F}t}{K} - \sum_{j=1}^{N} z_j^2\right)} \tag{3}$$

In the following, MD nanocompression simulations are performed at T=10 K using the Nosé-Hoover thermostat [20] and shrink-wrapped non-periodic boundary conditions. Atomic configurations are characterized using the Polyhedral Template Matching (PTM) method [21] and the Dislocation Extraction Algorithm (DXA) [22] as implemented in the Ovito software [23].

Figure 1 illustrates the mechanical response of a 14.57 nm Au faceted NP compressed at various loading rates ranging from 0.50 to 6.10 nN.ps^{-1} *i.e.,* $\dot{\varepsilon}$ $\sim$10^7-10^8 s^{-1} engineering strain rate, typical of classical MD simulations. In addition, a displacement-controlled simulation with $\dot{\Delta l}$=0.01

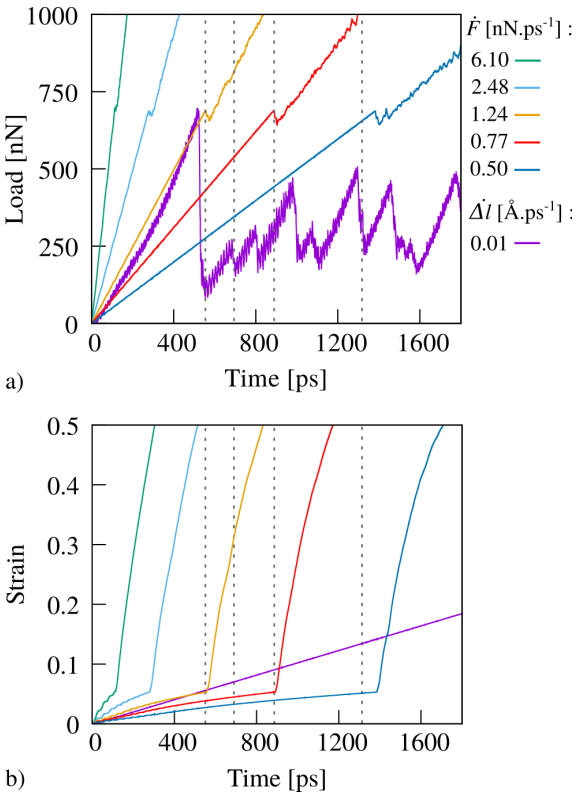

Figure 1: Mechanical response of a 14.57 nm height Au faceted NP under compression using load and displacement-controlled MD simulations. (a) Load *vs.* time, (b) engineering strain *vs.* time. Black dashed lines refer to time configurations illustrated in Figure 2.

	$\dot{F}$ [nN.ps^{-1}]					$\dot{\Delta l}$ [Å.ps^{-1}]
	6.10	2.48	1.24	0.77	0.50	0.01
F_y [nN]	698	688	690	689	687	689
σ_y [GPa]	8.80	8.67	8.70	8.69	8.66	8.69
t_y [ps]	113	280	555	890	1380	516
$\dot{\varepsilon}_e$ [10^8 s^{-1}]	4.73	1.89	0.94	0.59	0.38	1.03
$\dot{\varepsilon}_p$ [10^8 s^{-1}]	27.12	24.88	22.23	24.19	19.53	1.03
$\dot{F}_e$ [nN.ps^{-1}]	6.10	2.48	1.24	0.78	0.50	1.29
$\dot{F}_p$ [nN.ps^{-1}]	6.12	2.51	1.29	0.87	0.59	-

Table 1: Yield force F_y, critical stress and time σ_y and t_y as well as adjusted elastic and plastic strains and load rates ($\dot{\varepsilon}_e$, $\dot{\varepsilon}_p$, $\dot{F}_e$ and $\dot{F}_p$) computed during MD compression simulations of a 14.57 nm heigt Au faceted NP using load or displacement-control (respectively labelled $\dot{F}$ and $\dot{\Delta l}$).

Å.ps^{-1} equivalent to $\dot{\varepsilon}$=1.03 10^8 s^{-1} is shown. As usual for the latter, two deformation regimes are easily recognizable including a quasi-linear elastic regime up to a yield force F_y=689 nN where a force drop marks the beginning of the plastic deformation regime. As shown in Figure 2, the onset of plasticity is related to Surface Dislocation Nucleation (SDN) and consecutive glide events that reduce the height of the NP along the compression axis and, as a consequence, reduce the force exerted by the indenter during displacement-controlled simulations. In the case of load-control, the force also initially increases linearly following the imposed load-rate during elastic deformation before a rate-dependent load dip occurs, followed by a reload of the indenter force. For the displacement-controlled case, the engineering strain monotonically increases with time as a consequence of the imposed displacement rate whereas a rate-discontinuity is apparent at the load dip for force-controlled compression tests. It should be noted here that lowering the imposed displacement rate closer to experimental conditions might also induce strain-rate singularities. Details on critical values and rates before and after the load dip are provided in Table 1.

The sample shape and dislocation microstructure for the two simulations $\dot{F}$=1.24 nN.ps^{-1} and $\dot{\Delta l}$=0.01 Å.ps^{-1} are compared in Figure 2. For the displacement-controlled simulation, the first SDN event happens at t=516 ps with the nucleation of a $\frac{1}{6}[1\bar{2}\bar{1}](\bar{1}\bar{1}1)$ Shockley partial dislocation. Then,

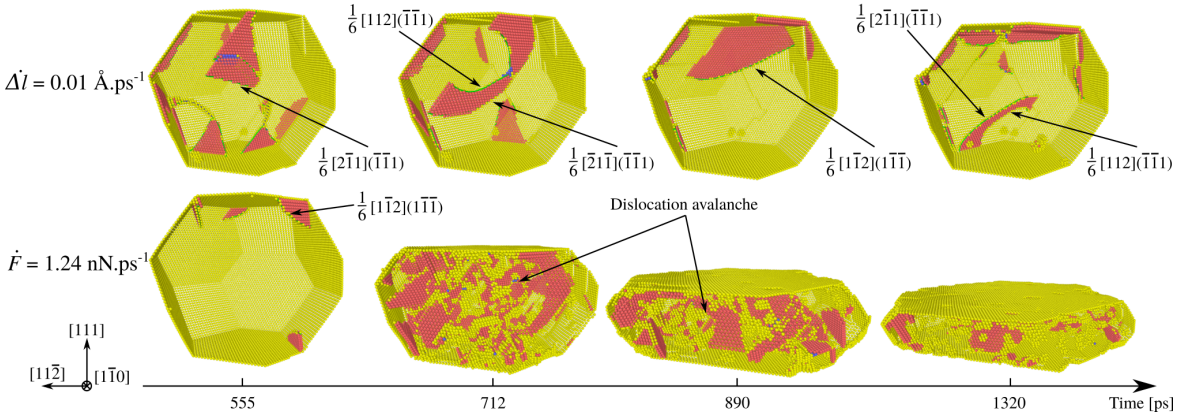

Figure 2: Shape and dislocation microstructure evolution of a 14.57 nm height Au faceted NP under compression using load and displacement-controlled MD simulations. Atoms colored in gold and red respectively refer to surfaces and stacking-fault environments. Shockley partial dislocations are illustrated by green curves.

the kinetics of the SDN process is particularly smooth in this case as dislocations nucleate in an uncorrelated manner. On the other hand, the first plastic event occurs at t=555 ps for the load-controlled compression and is followed by a strain burst made of numerous SDN events clustered in a very short time. These results reproduce and explain the sudden collapse of NPs (the "pancake" shape [24]) commonly observed in compression experiments using load-controlled or pseudo displacement-controlled setups (see *e.g.,* refs. [24, 6]), in contrast to more gradual shape changes observed in true displacement-controlled NP compression tests (*e.g.,* refs. [7, 8]).
Dislocation density ρ profiles (Figure 3a) show (i) load-controlled case: a ρ burst when the sample yields followed by a drop of a factor two. Only a slight dependence on the load rate is noticed in the investigated conditions of deformation which is consistent with the constant F_y behaviour. Finally, ρ reaches a steady state of about 1-3 10^{17} m^{-2}, (ii) displacement-controlled case: ρ is lower than in load-controlled simulations but continuously increases up to 4 10^{16} m^{-2}. Unlike load-controlled simulations, significant jumps and drops of ρ are observed when the displacement is controlled. They characterize discrete dislocation nucleation and exhaustion events as shown in Figure 2.
Also, the mean dislocation velocity $\bar{v}$ is obtained using the Orowan's equation $\dot{\varepsilon} = m\rho b\bar{v}$ where m=0.314 is the maximum Schmid factor for partial

dislocation slip systems assuming a compression axis along [111] and a partial dislocation Burgers vector b=1.66 Å (Figure 3b). The first point is that $\bar{v}$ is lower than the speed of the acoustic wave in Au ($\sim$3200 m.s^{-1}) and, more broadly, does not saturate whatever the control mode [25, 26, 27, 28]. For load-controlled simulations, $\bar{v}$ is characterized by a peak when the first dislocation nucleates ranging from 253 to 405 m/s and then settles in the 90 to 170 m/s range except for the lowest load-rate $\dot{F}$=0.50 nN/ps that shows a continuous increase of $\bar{v}$ conditioned by a singular decrease of ρ. In the displacement-controlled case, $\bar{v}$ reaches a maximum of $\sim$180 m/s before it significantly decreases down to a steady-state regime at about $\sim$70 m/s. Here we note that $\bar{v}$ is constrained by the strain rate which is about 25$\times$ lower in displacement-controlled than in load-controlled simulations in the plastic deformation regime (see Table 1).

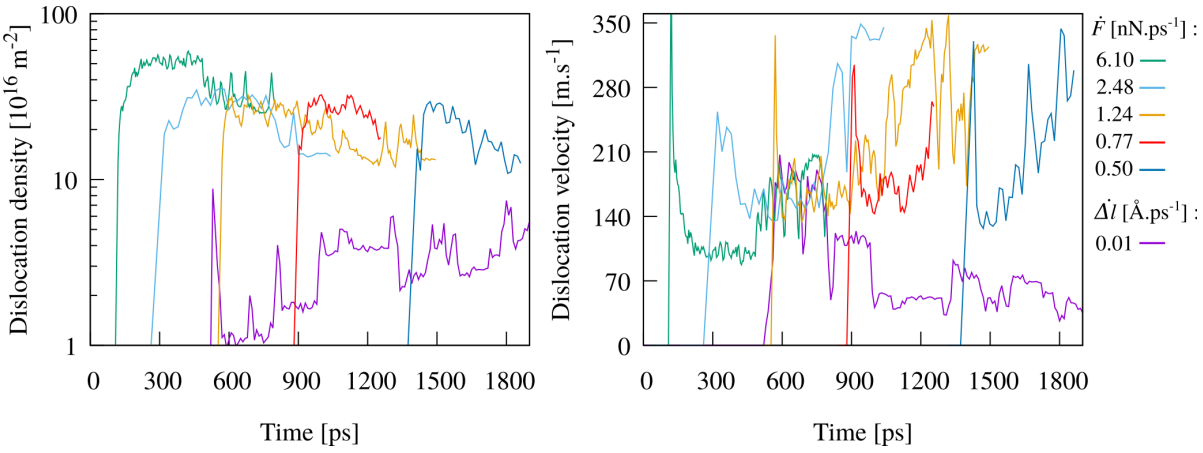

Figure 3: Dislocation density and velocity in a 14.57 nm height Au faceted NP under compression using load or displacement-controlled MD simulations. (a) Dislocation density and (b) Average dislocation velocity.

Whatever the control mode, the first SDN event leads to a global weakening of the NP *i.e.,* the NP is characterized by more numerous defects (surface ledges, dislocations) after the first SDN event than before. Therefore, this softens the energy landscape for the subsequent nucleation events, as confirmed by the lower amplitude of the secondary force peaks in Figure 1. While the softening of the sample is offset by the load drop in the displacement-controlled case, it has dramatic consequences under load-control where the

compressive force monotonically increases with time: the sample is pushed harder while becoming softer. As a consequence, the NP spontaneously collapses into a flat pancake shape due to the burst of dislocations in a very different manner than in the displacement-controlled case that is characterized by intermittent peaks and drops of the dislocation density (Figure 3a). The changes in terms of dislocation dynamics between the load- and displacement-controlled setups are confirmed in Figure 4 that shows engineering compressive stress *vs.* strain curves for Au faceted NP with size ranging from 7.52 to 22.56 nm, in the same interval than in the original work of Mordehai *et al.* [5, 11]. As shown in Figure 4, the computed yield stress σ_y increases with decreasing size which leads to smaller NPs being stronger than larger ones. These results quantitatively corroborate Mordehai *et al.* original MD results on the yield stress and nucleation processes. However, we show using our load-controlled MD setup that it becomes possible here to catch the sudden strain bursts originally observed in Mordehai *et al.* [5] nanocompression experiments but lacking in their displacement-controlled MD simulations.

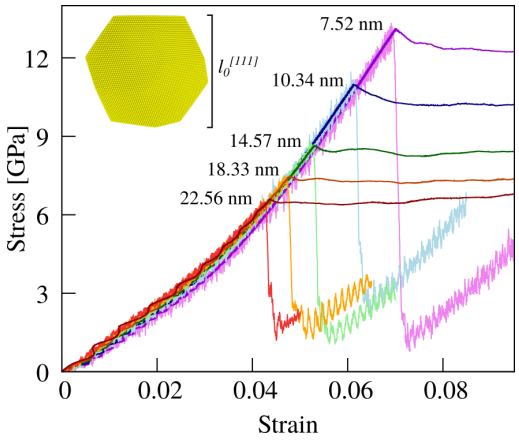

Figure 4: Stress-strain curves for Au faceted NPs of various size $l_0^{[111]}$ under compression computed using load ($\dot{F}$=0.77 nN.ps^{-1}, dark-colored curves) and displacement-controlled ($\dot{\Delta l}$=0.01 Å.ps^{-1}, light-colored curves) MD simulations.

To compare the mechanical response computed in displacement-controlled MD to those derived from load-controlled or pseudo displacement-controlled experiments, several research groups assume an envelope load model that connects load maxima. To confront this hypothesis to our load-controlled

MD protocol, we reproduced the virtual compression experiments of Sharma *et al.* [13] on 20.1 nm Ag hemispheres using both our load and displacement-controlled protocols. Due to the similar conditions of simulation, our displacement-controlled simulation perfectly reproduces Sharma *et al.* results (Figure 5). The stress response is characterized at the beginning by an elastic regime that yields at about F_y=122 nN where SDN starts, the rest of the curve being made of classical MD load/unload cycles marked by subsequent nucleation events. The load envelope model connects the first load peak at critical displacement δ_y=2.80 Å to the next elastic reload (at displacement δ=4.17 Å), mimicking an experimental burst of deformation. Then, the model follows a classical peak-to-peak behaviour. One can notice that the NP initially strengthens here due to its hemispherical shape that constrains the evolution of the contact area and stress heterogeneities. Load-control simulation results show a similar elastic trend with the first SDN event occurring at F_y=122 nN and δ_y=2.75 Å. As confirmed by the envelope load model, a displacement jump up to δ=3.96 Å is observed in the load-controlled simulation, after the first SDN event. However, the MD simulation and the model diverge after δ=4.04 Å. To interpret this change in the mechanical response, we reveal the atomic structure of both NPs at this stage in Figure 5. While the displacement-controlled simulation shows a defect-free sample, the load-controlled simulation exhibits a well-established dislocation microstructure made of Shockley partial dislocations and extended stacking-faults. So, on one hand, an elastic reload up to high-stress is necessary to further plastically deform a defect-free sample via SDN (displacement-controlled case) while, on the other hand, a stress plateau is at the roots of a dislocation microstructure that has to be disorganized to carry on further the deformation (load-controlled case). As in the case of the Au faceted NPs discussed above, the larger amount of defects in the load-controlled case (for the same strain level as in the displacement-controlled case) is attributed to stress steady-state meanwhile the displacement-controlled simulation shows load relaxation. We conclude that the envelope load model is not able to quantitatively reproduce a load-controlled test as it does not account explicitly for the dislocation microstructure that drastically evolves during strain bursts.

To conclude, load-controlled MD simulations allow to draw a more comprehensive picture of nanomechanical experiments and simulations. Indeed, at variance with usual displacement-controlled atomistic simulations, load-controlled simulations show strain bursts more akin to those observed in

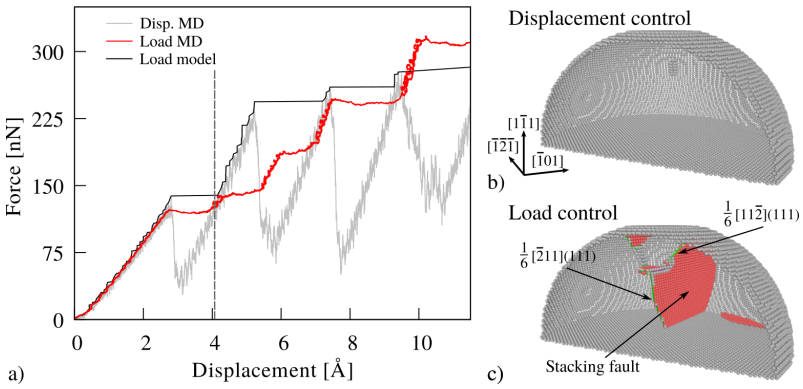

Figure 5: MD nanocompression simulation of a 20.1 nm Ag half-sphere using load and displacement-controlled MD. (a) Force *vs.* displacement curves computed using load-controlled MD (Load MD), displacement-control (Disp. MD) and the envelope load model (Load model), (b, c) evolution of the dislocation microstructure at displacement $\delta = 4.04$ Å for the displacement and load-control cases, respectively.

NPs or pillars experiments when compressed inside the SEM [24, 29]. Both control modes are characterized by different dislocation dynamics and time-dependent microstructures which make their comparison difficult. When applied to NPs, load-controlled MD simulations provide a clear explanation for the often observed magic collapse of metal NPs, which has nothing to do with a nanoscale property of metals but rather relies on the (load-controlled) experimental setup used. Load-controlled MD provides an improved basis for better interpretations of nanomechanics experiments where it could be applied to other types of tests than compression, as *e.g.,* in the case of nanoindentation simulations [30, 31].

Acknowledgements

This work was supported by the Agence National de Recherche, grant no. ANR-20-CE09-0015 (ANR SASHA) and the HPC resources (P2CHPD) of the Fédération Lyonnaise de Modélisation et Sciences Numériques (FLMSN). The authors acknowledge Pr. E. Rabkin and the Plasticité 2022 community for useful discussions.

References

[1] K. Hemker, W. Sharpe Jr., Materials Research 37 (2007) 93–126.

[2] M. Legros, Comptes Rendus Physique (2014) 1 – 17.

[3] O. L. Warren, S. A. Downs, T. J. Wyrobek, Zeitschrift für Metallkunde 95 (2004) 287–296.

[4] G. Dehm, B. Jaya, R. Raghavan, C. Kirchlechner, Acta Materialia 142 (2018) 248–282.

[5] D. Mordehai, M. Kazakevich, D. J. Srolovitz, E. Rabkin, Acta Materialia 59 (2011) 2309–2321.

[6] W.-Z. Han, L. Huang, S. Ogata, H. Kimizuka, Z.-C. Yang, C. Weinberger, Q.-J. Li, B.-Y. Liu, X.-X. Zhang, J. Li, E. Ma, Z.-W. Shan, Advanced Materials 27 (2015) 3385–3390.

[7] I. Issa, J. Amodeo, J. Réthoré, L. Joly-Pottuz, C. Esnouf, J. Morthomas, M. Perez, J. Chevalier, K. Masenelli-Varlot, Acta Materialia 86 (2015) 295 – 304.

[8] I. Issa, L. Joly-Pottuz, J. Amodeo, D. J. Dunstan, C. Esnouf, J. Réthoré, V. Garnier, J. Chevalier, K. Masenelli-Varlot, Materials Research Letters 9 (2021) 278–283.

[9] D. Mordehai, O. David, R. Kositski, Advanced Materials 30 (2018) 1706710.

[10] J. Amodeo, L. Pizzagalli, Comptes Rendus. Physique 22 (2021) 1–32.

[11] Y. Feruz, D. Mordehai, Acta Materialia 103 (2016) 433 – 441.

[12] R. Kositski, O. Kovalenko, S.-W. Lee, J. R. Greer, E. Rabkin, D. Mordehai, Scientific Reports 6 (2016) 25966 – 8.

[13] A. Sharma, J. Amodeo, N. Gazit, Y. Qi, O. Thomas, E. Rabkin, ACS Nano 15 (2021) 14061.

[14] A. P. Thompson, H. M. Aktulga, R. Berger, D. S. Bolintineanu, W. M. Brown, P. S. Crozier, P. J. i. t. Veld, A. Kohlmeyer, S. G. Moore, T. D. Nguyen, R. Shan, M. J. Stevens, J. Tranchida, C. Trott, S. J. Plimpton, Computer Physics Communications 271 (2022) 108171.

[15] G. Grochola, S. P. Russo, I. K. Snook, The Journal of Chemical Physics 123 (2005) 204719.

[16] X. W. Zhou, R. A. Johnson, H. N. G. Wadley, Physical Review B 69 (2004) 144113.

[17] J. Rahm, P. Erhart, Journal of Open Source Software 5 (2020) 1944.

[18] P. Hirel, Computer Physics Communications 197 (2015) 212–219.

[19] J. Amodeo, K. Lizoul, Materials and Design 135 (2017-12) 223 – 231.

[20] S. Nosé, Molecular Physics 52 (1984) 255 – 268.

[21] P. M. Larsen, S. Schmidt, J. Schiøtz, Modelling and Simulation in Materials Science and Engineering 24 (2016) 055007 – 19.

[22] A. Stukowski, K. Albe, Modelling and Simulation in Materials Science and Engineering 18 (2010) 085001.

[23] A. Stukowski, Modelling and Simulation in Materials Science and Engineering 18 (2010) 7pp.

[24] D. Mordehai, S.-W. Lee, B. Backes, D. J. Srolovitz, W. D. Nix, E. Rabkin, Acta Materialia 59 (2011) 5202 – 5215.

[25] B. Gurrutxaga–Lerma, J. Verschueren, A. P. Sutton, D. Dini, International Materials Reviews 66 (2021) 215–255.

[26] H. Tsuzuki, P. S. Branicio, J. P. Rino, Acta Materialia 57 (2009) 1843–1855.

[27] J. Marian, A. Caro, Physical Review B 74 (2006) 024113.

[28] I. Bryukhanov, International Journal of Plasticity 135 (2020) 102834.

[29] J. Greer, W. Oliver, W. Nix, Acta Materialia 53 (2005) 1821 – 1830.

[30] G. Ziegenhain, H. M. Urbassek, A. Hartmaier, Journal of Applied Physics 107 (2010) 061807.

[31] C. Begau, A. Hartmaier, E. P. George, G. M. Pharr, Acta Materialia 59 (2011) 934 – 942.